BULLETIN OF THE POLISH ACADEMY OF SCIENCES
TECHNICAL SCIENCES
Vol. 56, No. 1, 2008

Frequency sampling approach to the problem of silicon integrated spiral inductors modeling

M. KAŁUŻA* and A. NAPIERALSKI

Department of Microelectronics and Computer Science, Technical University of Lodz,
11 Politechniki Ave., 90-924 Łódź, Poland

Abstract. The aim of this paper is to present a new approach to the problem of silicon integrated spiral inductors modeling. First, an overview of models and modeling techniques is presented. Based on 3D simulations and published measurement results, a list of physical phenomena to be taken into account in the model is created and based on it, the spiral inductor modeling by frequency sampling method is presented. To verify the proposed method a test circuit, containing 6 spiral inductors was designed and integrated in a silicon technology. The parameters of the spiral inductors from the test circuit were next measured and compared with simulations results. The comparison for one of those six spiral inductors is presented in the article.

Key words: silicon integrated spiral inductors, MIS microstrip, inductance.

1. Introduction

The silicon-integrated spiral inductors have been almost forgotten in the 1960's after the publication in the United-States of R.M. Warner's book [1] stating that this components, integrated in silicon technologies have unacceptable parameters, especially low inductance values L and low quality factors Q: "Inductors with practical values of inductance and Q are by far the most difficult components to fabricate by integrated circuit techniques... it seems likely that any necessary inductance will be placed external to the monolithic circuit". It was necessary to wait until 1990 and the publication by Nguyen [2] of "Si IC-compatible inductors and LC passive filters" to bring back the attention of the scientific community to the forgotten spiral rectangular inductors in silicon technologies. Today, spiral inductors are widely used in RF circuits, for example in mobile communication systems.

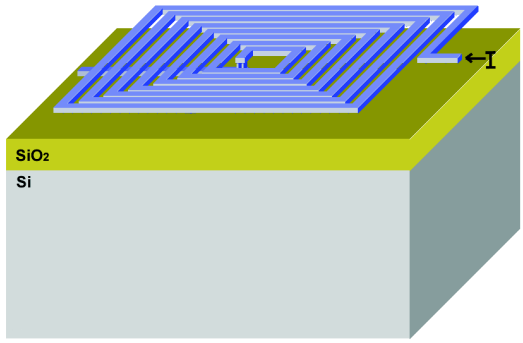

Fig. 1. Silicon-integrated spiral inductor

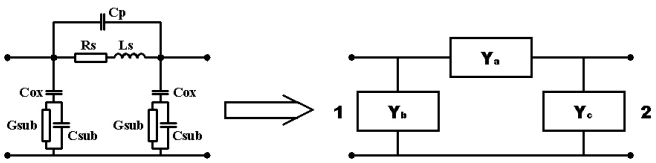

Fig. 2. 9-element spiral inductor Π model

2. Related work

2.1. The simple model. The model the most frequently used to represent a silicon integrated spiral inductor is the 9-element model (see Figs. 1, 2). It is based on MIS microstrip equivalent circuits [3]. In Fig. 2, the resistance R_S represents the series resistance of the spiral, inductance L_S – series inductance of the spiral and two C-GC branches are describing the semiconductor substrate, as proposed by Hasegawa [3]. The capacitance C_{OX} models the silicon dioxide capacitance and the parallel connection of capacitance C_{sub} and conductance G_{sub} is modeling the silicon substrate. C_p represents the interwinding capacitance. The values of the elements building the Π model can be calculated from the 2-port measurements of a spiral inductor. For a 2-port admittance matrix we have:

$$\bar{Y} = \begin{bmatrix} \bar{y}_{11} & \bar{y}_{12} \\ \bar{y}_{21} & \bar{y}_{22} \end{bmatrix} \tag{1}$$

$$\bar{Y}_a = \bar{y}_{11} + \bar{y}_{12} \tag{2}$$

$$\bar{Y}_b = -\bar{y}_{12} \tag{3}$$

$$\bar{Y}_c = \bar{y}_{12} + \bar{y}_{22}. \tag{4}$$

From the equations above, it is obvious that the 9-element Π model can accurately represent a spiral inductor for a giv-

*e-mail: mkaluza@poczta.onet.pl

en frequency point. If the spiral inductor parameters are frequency dependent, the Π model will loose its accuracy and it would be possible to use it only as a narrow-band model or a model acceptable in the frequency range, in which the inductor parameters changes are small. What is more, a spiral inductor, being in fact an on-chip interconnect, when integrated in a silicon technology, should be approached as a MIS microstrip [3], a MIS spiral inductor. It implies, that depending on the value of the silicon substrate resistivity and on the frequency of operation, the structure behavior will be different. When the product of the substrate resistivity and frequency will be large enough, the substrate will act as a dielectric, the structure could be regarded as a structure with a two-layer dielectric and the mode of propagation will be quasi-TEM. When the product of the substrate resistivity and frequency will be small enough, the substrate will act as a high loss conductor, thus the MIS spiral inductor could be in such a case regarded as an interconnect on an imperfect ground plane, made of silicon. The mode of propagation will be the so-called skin-effect mode. When the frequency is not so high and the resistivity of the substrate is moderate, typical for commercial silicon technologies, the type of propagation will be slow-wave mode, with a strong polarization of the Si-SiO_2 interface and a reduction of the propagated wave velocity. The effective permittivity of the silicon dioxide layer will increase and the electric field energy will be practically enclosed in the SiO_2 layer, which will lead to the increase of the capacitance between the spiral inductor and the substrate.

From above, it is clear that a simple Π model will not be able to represent several frequency dependent physical phenomena, occurring in a silicon integrated spiral inductor:

- spiral series resistance changes, related to the skin and proximity effects,
- spiral series inductance changes, related to the eddy currents generated in the silicon substrate, especially in the frequency-substrate resistivity range, were the mode of propagation is the skin-effect mode,
- substrate losses,
- substrate capacitance and resistance changes, related to the shift from slow-wave mode of propagation to the quasi-TEM or the skin-effect mode of propagation,
- transmission effects, which could appear in electrically long spirals, especially when slow-wave propagate.

As a result of those limitations of the simple, yet generally inaccurate 9-element Π model, different improvements were proposed. In [4, 5], the authors added a lateral substrate branch, to capture the additional effects of displacement and conduction currents flowing through the substrate. In [6–8], the possibility of using transformer loops was investigated, to incorporate the effects of frequency-dependent series loss in spiral inductors, achieving high accuracy over a wide frequency range, in particular for spiral inductors on low resistivity substrates, where eddy-current loss in the substrate is dominant [7, 8]. In [9], ladder networks were used, to account for the frequency dependent series spiral losses.

The limitations of the single Π network topology are becoming apparent, as the physical size of the spiral becomes electrically larger and distributed trends are becoming visible as a decrease in the effective series resistance of the spiral at higher frequencies, even to negative values. Thus in [5, 7, 8] 2Π models, consisting of two cascaded Π sections were proposed. In [10, 11], the 2Π concept was further extended. The authors represented the spiral using a chain of elementary Π cells, coupled inductively and capacitively, where one cell represented one segment of the spiral. The RLC building elements of each cell were calculated using closed form expressions. They were all frequency independent and thus, this approach suffered of almost the same problems in capturing frequency dependent characteristics of the spiral, as the simple 9-element Π model.

2.2. Impact of spiral inductor geometry on its series resistance. Silicon integrated spiral inductors can be designed as circular or rectangular ones. For technological reasons, most of the time, rectangular geometry is used (see Fig. 1). A rectangular spiral inductor geometry can be considered as a series of mutually parallel segments of on-chip interconnects. Its geometry can be described using 6 parameters: t – interconnect thickness, w – segments width, s – segments edge-to-edge distance, l_1 – length of the first segment, l_2 – length of the second segment and z – total number of segments. An additional segment is connecting the center of a spiral inductor with outside circuits.

To asses the impact of the spiral inductor geometry and substrate resistivity on the spiral inductor parameters, a series of 3D full-wave simulations was conducted. Special attention was paid to the problem of spiral geometry impact on the inductor series resistance R_s, taking especially into account the skin effect and the proximity effects.

The skin effect leads to an uneven distribution of current density flowing trough the conductor, which, with the increase of the frequency, is pushed to the conductor surface. The skin depth is the depth at which the current density is reduced to 1/e. It can be calculated using Eq. (5):

$$\delta = \frac{1}{\sqrt{2\Pi f \mu \sigma}} \tag{5}$$

where δ is the skin depth, σ is the conductor conductivity and μ, magnetic permeability.

As example, for aluminum and copper interconnects, the skin depth at the frequency of 10 GHz is equal to 0.82 μm and 0.65 μm respectively. Because in submicron silicon technologies, the thickness of on-chip interconnects usually does not exceed 1 μm, one can assume that for frequencies below 10 GHz, the impact of the skin effect on series resistance of a spiral inductor can be neglected in the process of modeling and designing. One can assume that the series resistance of such inductor can be modeled using one, frequency independent resistance value, as in the simple Π model. However, it is not a general rule. In some CMOS or BiCMOS silicon technologies, a special interconnect layer is added, with metallization thickness of 4–5 μm, for global routing and spiral

inductor design [14]. In such a case, the skin effect cannot be neglected. Similarly, if 2 or more interconnect layers will be stacked together, in order to reduce the series resistance of the designed inductor.

To prove the assumption that it is possible, in most cases, to neglect the skin effect when modeling spiral inductors, a series of simulations was conducted. Unexpectedly, in some cases a strong increase of inductor series resistance was observed. The results of one of such series of 3D full-wave simulations are shown in Fig. 3.

Fig. 3. Impact of spiral windings separation on the series resistance of the spiral inductor (square spiral, first segment length $l_1 = 400$ μm, segments width $w = 5$ μm, interconnect thickness $t = 1$ μm, segments edge-to-edge distance s value was changed from 10 μm to 1 μm)

Simulations were conducted for a square spiral with a first segment length $l_1 = 400$ μm, segments width $w = 5$ μm and interconnect thickness $t = 1$ μm. During simulations the edge-to-edge distance between segments, described by the s parameter, was changed.

Because a spiral inductor is a series of parallel, closely spaced on-chip interconnect segments, the currents flowing in the spiral's adjacent segments can mutually influence each other, leading to current crowding. As shown in Fig. 3, reducing edge-to-edge distance between the segments of the spiral leads to the increase of inductor series resistance with frequency. For a value of $s = 10$ μm, thus for $s = 2w$, the resistance increases very slowly with frequency. For $s = 5$ μm, therefore for an $s = w$ case, the resistance increase is slightly bigger, than for the $s = 10$ μm ($s = 2w$) case. When reducing more the edge-to-edge distance s, the series resistance increase with frequency becomes quicker, more pronounced and appears at lower frequencies. The series resistance increase is visible at much lower frequencies that one would expect, taking into account only the skin effect. Those are the results of the proximity effects.

In Figs. 4a-d are shown the results of 3D simulations of a square spiral inductor with a first segment length $l_1 = 400$ μm, segments width $w = 10$ μm, segments edge-to-edge distance $s = 10$ μm and interconnect thickness $t = 1$ μm. With the increase of frequency, one can see the changes in current density distribution in the spiral inductor. For the frequency of 100 MHz (Fig. 4a) the current density distribution is almost uniform. For the frequency of 500 MHz (Fig. 4b) there are visible changes in current distribution. The current density is increasing on the sides of the spiral segments and is decreasing in the middle. With further increase of frequency, this effect is more pronounced. The non-uniform current density distribution appeared at lower frequencies, that one would expect from the skin effect. In the case of skin effect, the current flowing trough a conductor is pushed to its surface. In Figs. 4a-4d, one can clearly see, it is not the case, as the current is pushed to the sides of the conductors. Again, those are the results of the proximity effects.

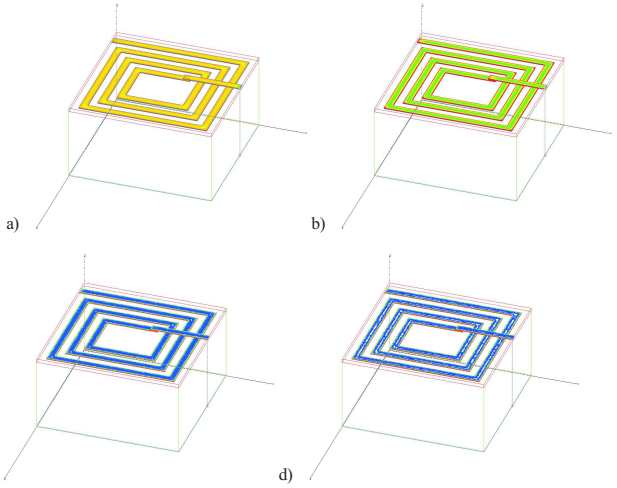

Fig. 4. Results of simulations showing the proximity effects – increase of current density on the edges of the spiral (a – 100 MHz; b – 500 MHz; c – 5 GHz; d – 10 GHz)

The results shown in Figs. 3 and 4 are very important. In some publications, the authors advise, as a mean of optimization of spiral inductor geometry and a way to maximize its quality factor Q, to reduce the edge-to-edge distance s of the spiral to the lowest possible value, allowed by the technology rules. Taking into account the results shown above, such an approach should be unambiguously considered as a design error.

2.3. Impact of eddy currents on spiral inductor series resistance. In [20] the authors suggested, based on a simulation of a simplified spiral inductor structure, the possibility of a bigger increase of series resistance of internal segments of a spiral inductor, comparing to the external segments of the spiral. They stated, that the increase in magnetic flux density in the spiral axis would lead to the generation of eddy currents in the spiral. From results shown in Fig. 5, one can see, that for the frequency of 2 GHz, the resistance increase for the outside segment is only 18%, whereas for inside segment is 480%, comparing to DC values.

To verify the impact of eddy currents on spiral inductors, own full-wave 3D electromagnetic simulations were conducted. An example result, for a square 140×140 μm spiral inductor is shown in Fig. 6. The local increase of magnetic flux density inside the spiral inductor is clearly visible. If any on-chip interconnects would be routed through that area, their series resistance would increase with the increase of the fre-

quency much faster, than just taking into account the skin or proximity effects. One can therefore state, that when designing spiral inductors, the inside of the spiral should be free, leaving the spiral geometry hollow, especially given the fact, that inside spiral segments are contributing little to the overall inductance value of the spiral inductor (see Fig. 7).

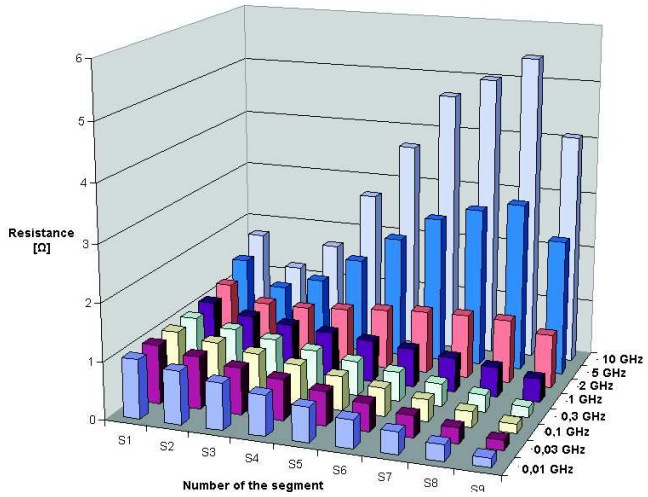

Fig. 5. Change of spiral inductor segments series resistance vs. frequency after Ref. 20

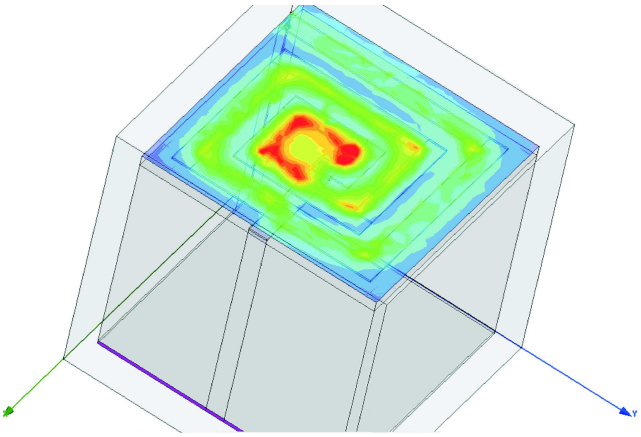

Fig. 6. Results of 3D electromagnetic simulation of a small, 140×140 μm spiral inductor

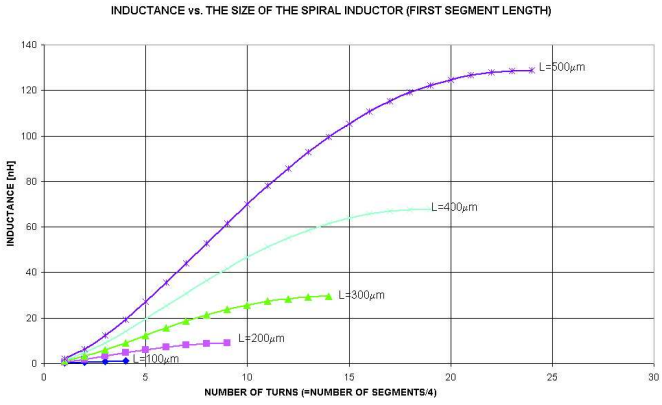

Fig. 7. Spiral inductor inductance in function of the number of segments

3. Algorithm of inductor modeling by frequency sampling

3.1. General idea. First, based on a series of extensive, full-wave 3D FDTD electromagnetic simulations and on published measurements data, a list of physical phenomena to be accounted for when modeling silicon integrated spiral inductors was created. Those physical phenomena are:

- spiral resistance related to the finite conductivity of the spiral,
- skin effect,
- proximity effect,
- losses related to the eddy currents generated in the silicon substrate,
- spiral series inductance,
- silicon dioxide capacitance,
- silicon substrate conductance and capacitance,
- interwinding capacitances,
- silicon substrate properties change, related to the transition from slow-wave mode to the skin-effect or quasi-TEM modes of propagation,
- transmission effects in electrically large spirals.

Two sets of data are the starting point of the calculation algorithm:

- technology data, including the thickness of different semiconductor and conductor layers, their spacing and parasitic resistances and capacitances of the given technology,
- data describing the spiral geometry.

The spiral is divided into segments. Its geometry can be described using 6 parameters (see Fig. 8): t – the trace thickness, w – the trace width, s – the edge-to-edge distance between segments, l_1 – the length of the first segment, l_2 – the length of the second segment and z – the total number of segments. An additional underpass segment is connecting the center of the spiral to the external circuits.

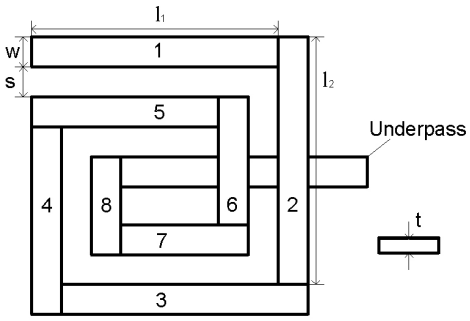

Fig. 8. Spiral geometry segmentation

Based on the data above, the spiral inductor will be described using a chain of elementary cells (see Fig. 9). For a z segment spiral, the chain will have z elementary cells. Contrary to [10, 11], the values of elementary cell elements are frequency dependent. This chain model represents the spiral inductor for only one given frequency point, thus for every frequency point in the frequency range of interest, there will be one chain circuit.

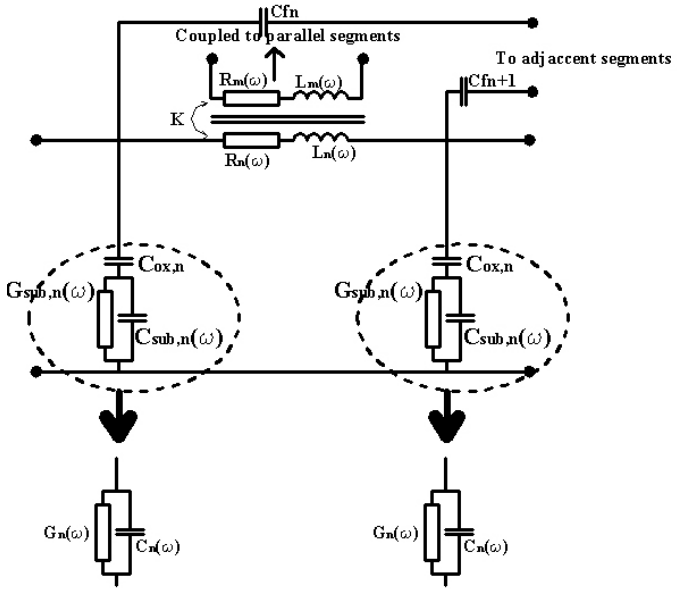

Fig. 9. Elementary cell representing one segment of a spiral inductor for one, given frequency

In Fig. 9, R_n is the n-th segment series resistance, L_n is the n-th segment series inductance, $C_{ox,n}$ silicon dioxide capacitance of the n-th segment, $C_{sub,n}$ is the silicon substrate capacitance of the n-th segment and $G_{sub,n}$ is the silicon substrate conductance of the n-th segment. Every of those elements is frequency dependent. Their value for a given segment will vary with frequency.

The values of resistances, capacitances and inductances for each elementary cell are calculated using readily available closed form expressions [10, 12–14]. To take into account the frequency dependence of silicon substrate behaviour in a MIS Si-SiO_2 multilayer structure, the equations developed and presented in [13] are used:

$$C(\omega) = \frac{\omega^2 C_{Si} C_{ox} (C_{Si} + C_{ox}) + C_{ox} G_{Si}^2}{G_{Si}^2 + \omega^2 (C_{Si} + C_{ox})^2} \tag{6}$$

$$G(\omega) = \frac{\omega^2 G_{Si} C_{ox}^2}{G_{Si}^2 + \omega^2 (C_{Si} + C_{ox})^2} \tag{7}$$

where $C(\omega)$ is the shunt capacitance of a microstrip and $G(\omega)$ is the shunt conductance of a microstrip (see Fig. 9).

Using the concept of the effective complex height of a MIS microstrip [14], it is possible to take into account the substrate losses related to the eddy currents generated in the silicon layer.

$$h_{eff} = h_{ox} + \frac{1-j}{2} \delta \tanh\left[(1+j)\, h_{sub}/\delta\right] \tag{8}$$

where h_{ox} is the SiO_2 layer thickness, h_{sub} is the Si layer thickness and δ the skin depth of the silicon.

To include the skin and especially the proximity effects in the spiral, the SRM method (Surface Ribbon Method) [15, 16] is used. The spiral geometry is divided into 2 cross-sections, X and Y, and for both sets of parallel segments the impact of skin and proximity effects on the series resistance of the spiral is calculated.

Next step of the algorithm, after building an elementary cell chain is to calculate the two-port **Y** admittance matrix of the circuit, using the modified nodal approach. This admittance matrix describes the spiral inductor for a given, single frequency point.

The entire procedure is repeated for the frequency range of interest. The end result is a series of two-port **Y** matrices, a set of frequency samples, describing the spiral inductor. This set of samples is similar to the results of a spiral inductor scattering parameters measurements, one can get using a vector network analyzer.

Using the algorithm given in [8, 17], this set of samples can be, in the next step, numerically transformed into a 2Π compact, wideband equivalent circuit, which can be used directly in a circuit solver.

The block algorithm of the spiral inductor frequency sampling method is shown in Fig. 10 below.

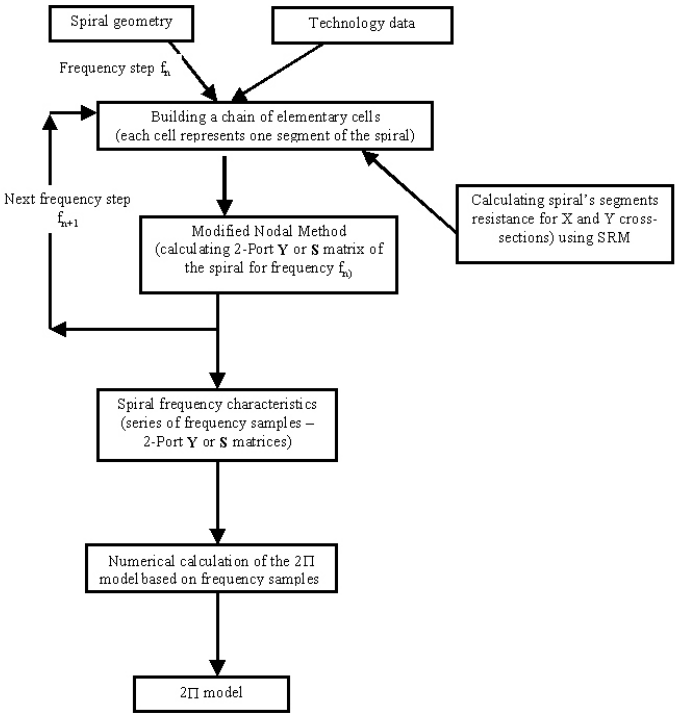

Fig. 10. Spiral inductor frequency sampling algorithm

The calculation times using the algorithm described above, for a 100 segment spiral, for one frequency point, at higher frequencies, on a PC with a 2.4 GHz Pentium 4 processor were exceeding 2 minutes. The main computational effort was coming from the SRM module. At higher frequencies more ribbons are required in the SRM method to represent each of the segments. To reduce the calculation time to seconds for a single frequency point, an approximate formula [18] can be used to calculate the resistance of the segments building the spiral. These equations are taking into account the skin effect as well as proximity effects.

$$R_{eff} = R_{DC}\left[1 + \frac{1}{10}\left(\frac{\omega}{\omega_{crit}}\right)^2\right] \tag{9}$$

$$\omega_{crit} = \frac{3.1 * (w+s)}{\mu_0 * w^2} R_{square} \tag{10}$$

where w is the trace width, s – the edge-to-edge distance between segments of the spiral, R_{DC} is the DC resistance, R_{square} is the resistance by square of the interconnect, given in the silicon technology file, ω_{crit} is the critical angular frequency and μ_0 is the free space magnetic permeability.

When building the frequency sampling algorithm, it was assumed, that the modeled spiral inductors are "hollow", that is, there are no segments filling the center of the spiral. If this condition is not met, it could lead at higher frequencies to an underestimation of the series resistance of the spiral and an overestimation of the spiral inductance and spiral quality factor.

3.2. Experimental results. To verify the proposed method, a CMOS test circuit containing spiral inductors was designed, fabricated (see Fig. 11), measured, and the results of those measurements were compared to the calculations made using the frequency sampling approach described above. The results of such comparison for one of those inductors ($t = 1.2$ μm, $w = 9$ μm, $s = 9$ μm, $l_1 = l_2 = 300$ μm, $z = 29$) are shown below. When calculating the model parameters, typical values of technology parasitic capacitances and resistances given in the design kit were used. As it can be seen in Figs. 12, 13 and 14, there is a good agreement between the measurement results and the calculation. The biggest error (23%) was observed in the calculation of the maximum value of the inductor quality factor. This can be explained by a lover test circuit interconnect resistance R_{square}, than the technology typical value, leading to an overestimation of the spiral resistance. Using a lover value of R_{square} would allow reducing that error.

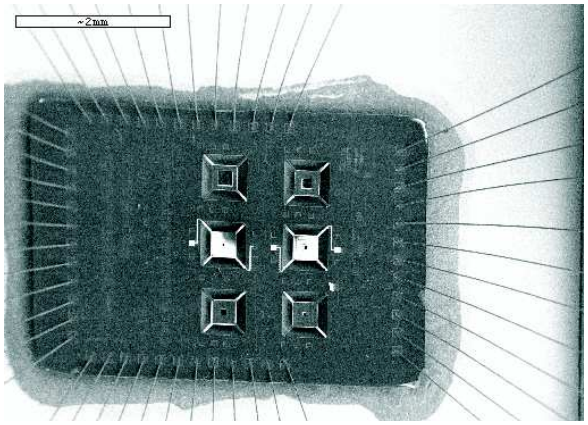

Fig. 11. The micromachined version of the BIOMI test circuit (only the standard, non-micromachined circuit parameters were measured

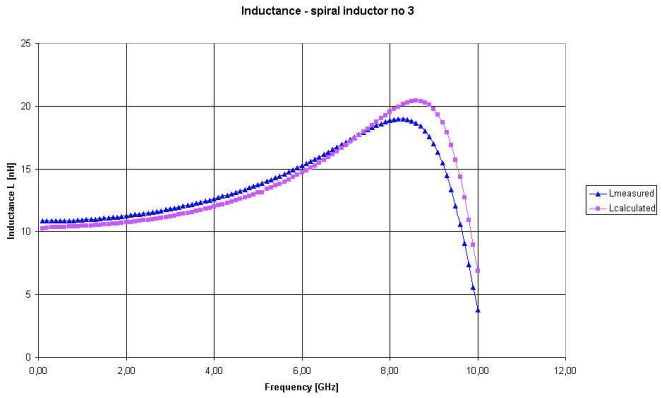

Fig. 12. Measured versus calculated spiral inductor inductance

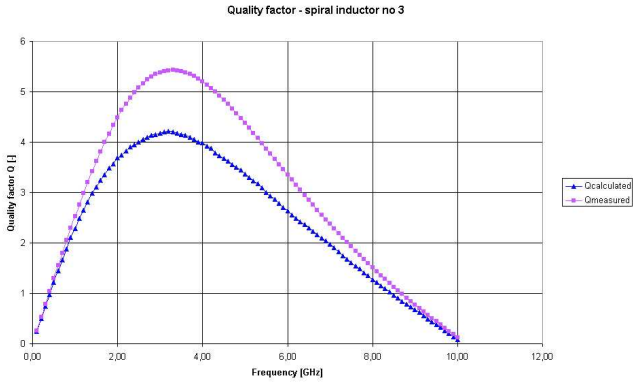

Fig. 13. Measured versus calculated spiral inductor quality factor

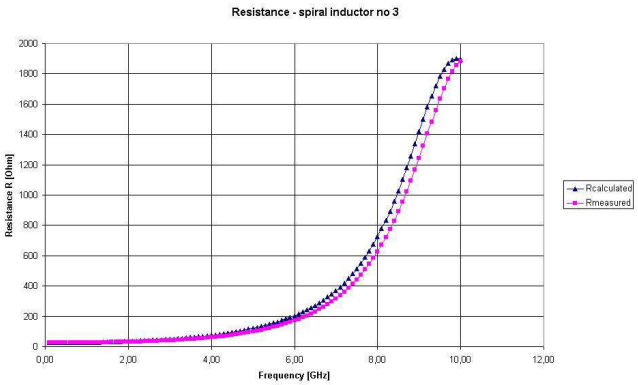

Fig. 14. Measured versus calculated spiral inductor resistance

To calculate the values of spiral inductor inductance L, quality factor Q and series resistance R from the two-port measurement results, Eqs. 11–13 shown below were used

- spiral inductor inductance

$$L = \frac{im\left[\frac{-1}{Y_{12}}\right]}{\omega} \tag{11}$$

- spiral inductor series resistance

$$R = re\left[\frac{-1}{Y_{11}}\right] \tag{12}$$

- spiral inductor quality factor

$$Q = \frac{im\,(Y_{11})}{re\,(Y_{11})}. \tag{13}$$

4. Conclusions

A novel approach to the problem of silicon integrated spiral inductors modeling, called the frequency sampling method was presented. The method transforms a complicated 3D problem into a set of two 2D cross sections. It allows capturing the frequency dependent characteristics of spiral inductors. Comparison is showing good agreement between measurements and simulations results. Differences between assumed technology parasitic capacitances and resistances and actual circuit values are source of error and should be checked during the design and modeling process. Slightly modifying the parasitic capacitances used in simulation, still remaining within the fast-slow technology data limits for parasitic capacitance and resistance values, would allow to further increase the accuracy of the simulations near the resonance frequency. The algorithm has an open structure and further physical effects could be easily added to it. It is also possible to simplify the proposed frequency sampling algorithm, if assuming, for example, that because of inductor geometry proximity of skin effects could be neglected.

The frequency sampling method was developed to model spiral inductors in silicon technologies, were three different modes of propagation, strongly influencing the inductor, has to be accounted for, but it can also be applied, after simplification, to other, non-silicon technologies.

Acknowledgements. I would like to thank prof. J. Dobrowolski and his staff for their valuable help in solving the problem of the spiral inductors measurements. My special thanks to prof. Etienne Sicard of GERME group, Institut National des Sciences Appliquées de Toulouse for his help in the realization of the integrated test circuit.

REFERENCES

[1] R.M. Warner, *Integrated Circuits: Design Principles and Fabrication*, McGrawHill, New York, 1965.

[2] N.M. Nguyen and R.G. Meyer, "Si IC-compatible inductors and LC passive filters", *IEEE J.f Solid State Circuits* 25 (8), 1028–1031 (1990).

[3] H. Hasegawa, M. Furukawa, and H. Yanai, "Properties of microstrip line on Si-SiO_2 system", *IEEE Trans. on Microwave Theory and Techniques* 19 (11), 869–881 (1971).

[4] J. Gil and H. Shin, "A simple wide-band on-chip Inductor model for silicon-based RF ICs", *IEEE Trans. Microwave Theory Techniques* 51 (9), 2023–2028 (2003).

[5] Y. Cao, R.A. Groves, X. Huang, N.D. Zamdmer, J.-O. Plouchart, R.A. Wachnik, T.-J. King, and C. Hu, "Frequency-independent equivalent-circuit model for on-chip spiral inductors", *IEEE J.l Solid-State Circuits* 38 (3), 419–426 (2003).

[6] W.B. Kuhn and N.K. Yanduru, "Spiral inductor substrate loss modeling in silicon RFICs", *IEEE RAWCON Proceedings*, 305–308 (1998).

[7] D. Melendy, P. Francis, C. Pichler, K. Hwang, G. Srinivasan, and A. Weisshaar, "Wide-band compact modeling of spiral inductors in RFICs", *IEEE MTT-S International Microwave Symposium Digest*, 717–720 (2002).

[8] A. Watson, P. Francis, K. Hwang, and A. Weisshaar, "Wide-band distributed modeling of spiral inductors in RFICs", *IEEE MTT-S International Microwave Symposium Digest*, 1011–1014 (2003).

[9] M. Kang, J. Gil, and H. Shin, "A simple parameter extraction method of spiral on-chip inductors", *IEEE Trans. on Electron Devices* 52 (9), 1976–1981 (2005).

[10] Y. Koustsoyannopoulos and Y. Papananos, "SISP: a CAD tool for simulating the performance of polygonal and multi-layer integrated inductors on silicon substrates", *Proceedings ICVC 97 Conference*, 244–246 (1997).

[11] Y.K. Koutsoyannopoulos and Y. Papanaos, "Systematic analysis and modeling of integrated inductors and transformers in RF IC design", *IEEE Trans. Circuits Syst. II* 47 (8), 699–713 (1998).

[12] H.M. Greenhouse, "Design of planar rectangular microelectronics inductors", *IEEE Transactions on Parts, Hybrids, and Packaging* 10 (2), 101–109 (1974).

[13] Hai Lan, *Analysis and Fast Extraction Technique for Microstrip On-Chip Interconnects on Silicon Substrate*, M.Sc. Thesis, Oregon State University, Corvallis, 2001.

[14] U. Arz, H. Grabinski and D. Williams, "Influence of the substrate resistivity on the broadband propagation characteristics of Silicon Transmission lines", *54^{th} ARFTG Conference Digest*, 58–63 (1999).

[15] S. Islam, *Modeling and Experimental Studies of Schottky-Contacted Coplanar Waveguide Transmission Lines on Semiconductor Substrates*, Ph.D. Thesis, University of Texas, Texas, 1994.

[16] E. Tuncer, *Extraction of Parameters of High-Speed Digital Interconnects*, Ph.D. Thesis, University of Texas, Texas, 1995.

[17] Watson, *Analysis and Modeling of Single-Ended and Differential Spiral Inductors in Silicon-Based RFICs*, M.Sc. Thesis, Oregon State University, Corvallis, 2003.

[18] William B. Kuhn and N.M. Ibrahim, "Approximate analytical modeling of current crowding effects in multi-turn spiral inductors", *Proceedings of the 2000 IEEE Radio Frequency Integrated Circuits (RFIC) Symposium*, 271–274 (2000).

[19] AT&T CBIC-V2 Bipolar Technology: press information 16/05/1995.

[20] J. Craninckx and M. Steyaert, "A CMOS 1.8-GHz low-phase-noise voltage-controlled oscillator with prescaler", *IEEE Journal of Solid State Circuits* 30 (12), 1474–1482 (1995).